AIAA JOURNAL
Vol. 41, No. 3, March 2003

Aeroelastic Dynamic Analysis of a Full F-16 Configuration for Various Flight Conditions

Philippe Geuzaine,* Gregory Brown,* Chuck Harris,† and Charbel Farhat‡
University of Colorado, Boulder, Colorado 80309-0429

An overview is given of recent advances in a three-field methodology for modeling and solving nonlinear fluid-structure interaction problems, and its application to the prediction of the aeroelastic frequencies and damping coefficients of a full F-16 configuration in various subsonic, transonic, and supersonic airstreams is reported. In this three-field methodology the flow is described by the arbitrary Lagrangian–Eulerian form of the Euler equations, the structure is represented by a detailed finite element model, and the fluid mesh is unstructured, dynamic, and updated by a robust torsional spring analogy method. Simulation results are presented for stabilized, accelerated, low-*g*, and high-*g* flight conditions, and correlated with flight-test data. Consequently, the practical feasibility and potential of the described computational-fluid-dynamics-based computational method for the flutter analysis of high-performance aircraft, particularly in the transonic regime, are discussed.

Nomenclature

b	=	body forces vector
$\boldsymbol{C}$	=	damping matrix
F, $\boldsymbol{F}$	=	continuous and discrete advective flux vector
f	=	aeroelastic frequency
$\boldsymbol{f}$	=	force vector
J	=	continuous Jacobian determinant $\mathrm{d}x/\mathrm{d}\xi$
$\boldsymbol{K}$	=	stiffness matrix
$\boldsymbol{M}$	=	mass matrix
n	=	normal vector
p	=	pressure
t	=	time
u, $\boldsymbol{u}$	=	continuous and discrete displacement fields
$\boldsymbol{V}$	=	control volume matrix
W	=	virtual work
w, $\boldsymbol{w}$	=	continuous and discrete fluid state fields
x, $\boldsymbol{x}$	=	continuous and discrete time-dependent position or displacement fields
α	=	aeroelastic damping
Γ	=	fluid-structure interface boundary
$\mathcal{E}$	=	energy transferred through Γ
ϵ	=	strain tensor
ξ	=	reference position
ρ	=	density
σ	=	stress tensor

Subscripts

F	=	value related to the fluid
S	=	value related to the structure
tor	=	value related to the torsion mode

Superscripts

ae	=	aerodynamic
ext	=	external
int	=	internal
n	=	time instance
P	=	predicted
$\cdot$	=	time derivative
$\hat{}$	=	virtual displacement quantity
$\tilde{}$	=	fictitious mechanical quantity

Received 18 June 2002; revision received 6 September 2002; accepted for publication 28 October 2002.

*Research Associate, Department of Aerospace Engineering Sciences, Center for Aerospace Structures. Member AIAA.

†Ph.D. Candidate, Department of Aerospace Engineering Sciences, Center for Aerospace Structures.

‡Professor, Department of Aerospace Engineering Sciences, Center for Aerospace Structures. Fellow AIAA.

I. Introduction

FLUTTER analysis is often conducted using the k,[1] p-k,[2] or other similar computational procedures based on the linear theory of aeroelasticity. Because they are fast and memory lean, these numerical algorithms are popular in the aerospace industry. In the subsonic regime most if not all of them rely on the doublet-lattice method[3] for computing the linear aerodynamic operator. This method, which was developed over 30 years ago, is still today the most used method for predicting subsonic unsteady flows in production environments. In the supersonic regime various methods related to the piston theory[4] are commonly used. However, high-performance military aircraft are usually flutter critical in the transonic speed range at high dynamic pressure. In this regime the mixed subsonic-supersonic flow patterns and shock waves are such that the linear flow theory in general, and therefore the doublet-lattice method in particular, is not reliable for predicting the unsteady aerodynamic forces acting on an aircraft. As a result, flutter testing of a scaled model in a transonic wind tunnel is always used to generate corrections to flutter speeds computed by linear methods. However, the design, construction, and testing of a wind-tunnel flutter model, and the analysis of the resulting data, require over a year's time.[5] For this reason, leading authorities in this field have recently suggested[5] that "The results of a finite number of [nonlinear] CFD (computational fluid dynamics) solutions could be used as a replacement for wind tunnel testing, assuming a validated code was available." This paper addresses this issue by first overviewing one among many CFD-based approaches that have been proposed for solving dynamic aeroelasticity problems (for example, see Refs. 6–11), then reporting on its application to the prediction, for various flight conditions, of the aeroelastic frequencies and damping ratios of a full fighter configuration.

The CFD and computational-structural-mechanics (CSM)-based aeroelastic code considered in this paper was developed at the University of Colorado. It relies on a three-field formulation of nonlinear fluid-structure interaction problems that is described in Sec. II of this paper and integrates advanced computational algorithms that are discussed in Sec. III. The focus fighter is an F-16 Block-40 aircraft in a clean wing configuration. Simulation results are presented in Sec. IV for various stabilized, accelerated, normal, loaded, subsonic, transonic, and supersonic flight conditions, and correlated with flight-test data provided by the Flight Test Center at Edwards Air Force Base (AFB). Finally, the practical feasibility and merit of

the described nonlinear solution methodology for extracting flutter envelopes in the transonic regime are addressed in Sec. V.

II. Three-Field Formulation of Nonlinear Aeroelastic Problems

A three-field formulation in the time domain of coupled fluid-structure interaction problems was introduced almost a decade ago[12] for modeling nonlinear dynamic aeroelasticity problems. This formulation is quite general. It can address many aeroelastic problems besides flutter, including the prediction of steady and unsteady loads, control surface effects in level flight and during maneuvering, aeroelastic tailoring, and performance analysis. In this formulation the aerodynamic forces acting on the structure are not predicted by the use of a linear aerodynamic operator because of the limitations associated with such an approach, particularly in the transonic regime. Rather, these unsteady forces are determined from the solution of the compressible Euler, or if necessary, Navier–Stokes equations. As recognized by another leading authority in this field,[13] there is a tendency to presume that most errors in an aeroelastic analysis are caused by inadequate aerodynamics, even though there are sufficient indications that in many cases the assumption of a linear structural behavior and the representation of this behavior by a truncated modal expansion contribute to the mismatch between prediction and flight test (see also Ref. 5). For this reason, in the three-field formulation overviewed in this paper the structure is not restricted to a harmonic motion with small displacement amplitudes and is not necessarily represented by a truncated basis of its normal modes. If necessary, nonlinear geometric, material, and free-play effects are properly accounted for. Furthermore, no restriction is imposed on the nature of the fluid-structure coupling, which is numerically modeled by suitable fluid-structure interface boundary (or transmission) conditions.

One difficulty in handling numerically the nonlinear fluid-structure coupling in the time domain stems from the fact that the structural equations are usually formulated with material (Lagrangian) coordinates, whereas the fluid equations are typically written using spatial (Eulerian) coordinates. Therefore, a straightforward approach to the solution of the coupled fluid-structure dynamic equations requires moving at each time step at least the portions of the fluid grid that are close to the moving and flexing aircraft. This can be appropriate for small displacements of the structure but can lead to severe grid distortions when it undergoes large motion. Different approaches have emerged as an alternative to partial regridding in transient aeroelastic computations, among which stand out the arbitrary Lagrangian–Eulerian (ALE) formulation[14] and the closely related method of dynamic meshes.[15] These approaches treat a computational aeroelasticity problem as a two-field coupled problem. However, a moving mesh can also be viewed as a pseudostructural (or fictitious structural) system with its own behavior,[12] and therefore, the coupled transient aeroelastic problem can be formulated as a three-rather than two-field problem: the fluid, the structure, and the dynamic fluid mesh. This three-field formulation has shed new light on the mathematical understanding of the numerical behavior of various algorithms applied to the solution of the coupled fluid-structure problem in the time domain and has enabled the development of faster solution algorithms.[7,16–18]

The simultaneous solution of the governing nonlinear fluid, fluid mesh, and structure equations of motion is computationally intensive and raises some concerns about the feasibility and practical usefulness of this approach in production environments. An important objective of this paper is to show that because of significant advances in computational methods and the advent of parallel processing the three-field and CFD-CSM-based solution of aeroelastic problems is now sufficiently mature and fast to be considered at least as a reliable simulation environment for addressing the critical flight conditions of a high-performance aircraft.

A. Governing Multidisciplinary Equations

A fluid-structure interaction problem can be described by the following coupled partial differential equations:

$$\left.\frac{\partial (Jw)}{\partial t}\right|_{\xi} + J\nabla_x \cdot \left[F(w) - \frac{\partial x}{\partial t} w\right] = 0 \tag{1a}$$

$$\rho_S \frac{\partial^2 u_S}{\partial t^2} - \operatorname{div}\left\{\sigma_S\left[\epsilon_S(u_S), \frac{\partial \epsilon_S}{\partial t}(u_S)\right]\right\} = b \tag{1b}$$

$$\tilde{\rho}\frac{\partial^2 x}{\partial t^2} - \operatorname{div}\left\{\tilde{\sigma}\left[\tilde{\epsilon}(x), \frac{\partial \tilde{\epsilon}}{\partial t}(x)\right]\right\} = 0 \tag{1c}$$

Equation (1a) is the ALE conservative form of the Euler equations. Here, $x(t)$ denotes the time-dependent position or displacement of a fluid grid point (depending on the context of the sentence and the equation), and $J = \det(\mathrm{d}x/\mathrm{d}\xi)$. Equation (1b) is the elastodynamic equation. Equation (1c) governs the dynamics of the moving fluid grid. It is similar to the elastodynamic equation because the dynamic mesh is viewed here as a pseudostructural system. A tilde notation is used to designate the fictitious mechanical quantities.[19] For the sake of notational simplicity, the various Dirichlet and Neumann boundary conditions intrinsic to each of the fluid and structure problems are omitted.

Equations (1a) and (1c) are directly coupled. If u_F denotes the ALE displacement field of the fluid and p its pressure field, Γ the fluid-structure interface boundary (wet boundary of the structure), and n the normal at a point to Γ, the fluid and structure equations are coupled by the transmission conditions

$$\sigma_S \cdot n = -pn \qquad \text{on} \qquad \Gamma \tag{2a}$$

$$\frac{\partial u_S}{\partial t} \cdot n = \frac{\partial u_F}{\partial t} \cdot n \qquad \text{on} \qquad \Gamma \tag{2b}$$

Equation (2a) states that the tractions on the wet surface of the structure are in equilibrium with those on the fluid side of Γ, whereas Eq. (2b) expresses the slip-wall boundary condition. The equations governing the structure and dynamic mesh motions are coupled by the continuity conditions

$$x = u_S \qquad \text{on} \qquad \Gamma \tag{3a}$$

$$\frac{\partial x}{\partial t} = \frac{\partial u_S}{\partial t} \qquad \text{on} \qquad \Gamma \tag{3b}$$

B. Semidiscretization of the Governing Equations

The spatial discretization of the ALE conservative form of the Euler equations by finite element (FE) or finite volume (FV) schemes leads to semidiscrete equations that can be written as

$$\dot{[\widehat{\boldsymbol{V}(\boldsymbol{x})\boldsymbol{w}}]} + \boldsymbol{F}(\boldsymbol{w}, \boldsymbol{x}, \dot{\boldsymbol{x}}) = 0 \tag{4}$$

where a bold font designates the discrete counterpart of a field variable. In the case of a FV semidiscretization, $\boldsymbol{V}$ is the matrix of the cell volumes, and $\boldsymbol{F}$ is the numerical convective flux approximating the integral of the physical flux function over the cell interfaces.

The semidiscretization by a FE method of the structural equations of dynamic equilibrium leads to

$$\boldsymbol{M}\ddot{\boldsymbol{u}}_S + \boldsymbol{f}_S^{\text{int}}(\boldsymbol{u}_S, \dot{\boldsymbol{u}}_S) = \boldsymbol{f}_S^{\text{ae}}(\boldsymbol{u}_S, \boldsymbol{w}) + \boldsymbol{f}_S^{\text{ext}} \tag{5}$$

where $\boldsymbol{M}$ is the FE lumped mass matrix. (This specific expression assumes that the rotational inertia forces are negligible.) If for the problem of interest the structure remains linear, Eq. (5) simplifies to

$$\boldsymbol{M}\ddot{\boldsymbol{u}}_S + \boldsymbol{C}\dot{\boldsymbol{u}}_S + \boldsymbol{K}\boldsymbol{u}_S = \boldsymbol{f}_S^{\text{ae}}(\boldsymbol{u}_S, \boldsymbol{w}) + \boldsymbol{f}_S^{\text{ext}} \tag{6}$$

Let the subscript i designate the grid points located in the interior of a computational domain and the subscript b designate those grid points located on the fluid-structure interface Γ. If the dynamic mesh is assimilated with a quasi-static pseudostructural system, the semidiscrete equation governing the evolution of the dynamic mesh can be written as

$$\tilde{\boldsymbol{K}}_{\text{ii}}\boldsymbol{x}_i = -\tilde{\boldsymbol{K}}_{\text{ib}}\boldsymbol{x}_b, \qquad \boldsymbol{x}_b = \boldsymbol{U}\boldsymbol{u}_{S_b} \tag{7}$$

where $\tilde{\boldsymbol{K}}$ is the fictitious time-dependent stiffness matrix resulting from the FE semidiscretization of Eq. (1c) (Ref. 19) and $\boldsymbol{U}$ is a transfer matrix. If the fluid and structure meshes have compatible interfaces, $\boldsymbol{U} = \boldsymbol{I}$. Otherwise, $\boldsymbol{U}$ is given by the FE discretization of Eq. (2b).

III. Computational Issues and Advances

In the linear theory of aeroelasticity, the air surrounding a flying aircraft can be interpreted as an "algebraic" damper whose sign depends on the flight conditions. When positive, it attenuates any aircraft vibration excited by some initial disturbance. When zero, it only entertains it, and when negative it amplifies that vibration. In other words, depending on the flight conditions and particularly the Mach number the air surrounding a vibrating aircraft can either extract energy from it, act as a neutral agent toward it, or feed it energy and cause it to flutter. This energy interpretation of the flutter mechanism underscores the importance of conserving as much as possible the energy transferred between the fluid and structure subsystems when discretizing the transmission conditions (2) and solving the coupled system of Eqs. (4), (5), and (7). Indeed, the extraction (transmission) from (to) the structure across the fluid-structure interface Γ of any significant amount of spurious numerical energy can artificially stabilize (destabilize) an otherwise unstable (stable) aeroelastic system.

Because the three-field aeroelastic problem (4), (5), and (7) is formulated in the time domain, extracting the wet frequencies and damping coefficients of the underlying structure for flutter analysis requires postprocessing the numerical output [for example, the displacement field $\boldsymbol{u}_S(t)$] by a parameter identification algorithm. Computational efficiency suggests using for this purpose an identification algorithm that requires as few cycles as possible of the predicted structural response. This in turn underscores the importance of producing a sufficiently accurate short window of the time response, and therefore time integrating this response by a scheme that is second-order time accurate for the coupled fluid-structure and not individual fluid and structure equations of motion (4) and (5). Usually, the aeroelastic response of the structure is dominated by its low modes. For this reason, computational speed favors implicit schemes and large computational steps, which underscores the importance of paying special attention to the numerical stability properties of the scheme designed for time integrating the coupled fluid-structure equations of motion.

A. CFD on Moving Meshes

The governing fluid equation (4) differs from the standard FE or FV semidiscretization of the Euler equations in that it is formulated on a moving rather than a fixed grid. Therefore, the time discretization of this equation, which incurs the approximation of the integral

$$\int_{t^n}^{t^{n+1}} \boldsymbol{F}(\boldsymbol{w}, \boldsymbol{x}, \dot{\boldsymbol{x}})\, \mathrm{d}t$$

raises the question of where to evaluate the convective fluxes when the grid moves from its position $\boldsymbol{x}^n$ at time t^n to a position $\boldsymbol{x}^{n+1}$ at time t^{n+1}. A straightforward answer to this question is to evaluate these fluxes on the mesh configuration $\boldsymbol{x}^n$ when the chosen time integrator is explicit and $\boldsymbol{x}^{n+1}$ when the time integrator is implicit. For small time steps $\Delta t^n = t^{n+1} - t^n$, it might not matter where the fluxes are evaluated because in that case the difference between the mesh configurations $\boldsymbol{x}^n$ and $\boldsymbol{x}^{n+1}$ might be insignificant. However, for the large time steps dictated by computational efficiency the method of evaluation of the integral

$$\int_{t^n}^{t^{n+1}} \boldsymbol{F}(\boldsymbol{w}, \boldsymbol{x}, \dot{\boldsymbol{x}})\, \mathrm{d}t$$

can have a dramatic effect on the performance of the time integration of Eq. (4). To address this issue, it was proposed in Refs. 7, 16, and 17 to first select a time integrator that performs well on fixed grids and then extend it to moving grids by evaluating a moving flux as the time average of a certain number of fluxes computed on a suite of carefully chosen mesh configurations. For example, the extension to moving grids of the classical three-point backward difference scheme, which is second-order time accurate on fixed grids, can be written as follows:

$$\alpha_{n+1}\boldsymbol{V}^{n+1}\boldsymbol{w}^{n+1} + \alpha_n \boldsymbol{V}^n \boldsymbol{w}^n + \alpha_{n-1}\boldsymbol{V}^{n-1}\boldsymbol{w}^{n-1} + \Delta t^n \sum_{s=1}^{n_s} c_s \boldsymbol{F}(\boldsymbol{w}^{n+1}, \boldsymbol{x}_s, \dot{\boldsymbol{x}}_s) = 0 \tag{8}$$

where

$$\alpha_{n+1} = (1+2\tau)/(1+\tau), \qquad \alpha_n = -1-\tau$$

$$\alpha_{n-1} = \tau^2/(1+\tau)$$

and $\tau = \Delta t^n / \Delta t^{n-1}$. Here, n_s denotes the number of mesh configurations, c_s the averaging weights, and $\boldsymbol{x}_s$ and $\dot{\boldsymbol{x}}_s$ denote the linear combinations of the mesh configurations $\{\boldsymbol{x}^{n-l}, \ldots, \boldsymbol{x}^n, \ldots, \boldsymbol{x}^{n+m}\}$ and velocities $\{\dot{\boldsymbol{x}}^{n-j}, \ldots, \dot{\boldsymbol{x}}^n, \ldots, \dot{\boldsymbol{x}}^{n+q}\}$, respectively, for some given integers l, m, j, and q.

The computational complexity of the scheme (8) can be reduced by averaging the mesh configurations themselves instead of the fluxes associated with them, which leads to

$$\alpha_{n+1}\boldsymbol{V}^{n+1}\boldsymbol{w}^{n+1} + \alpha_n \boldsymbol{V}^n \boldsymbol{w}^n + \alpha_{n-1}\boldsymbol{V}^{n-1}\boldsymbol{w}^{n-1} + \Delta t^n \boldsymbol{F}\left(\boldsymbol{w}^{n+1}, \sum_{s=1}^{n_s} c_s \boldsymbol{x}_s, \sum_{s=1}^{n_s} c_s \dot{\boldsymbol{x}}_s\right) = 0 \tag{9}$$

This alternative approach, which is the one selected in the present study, was proposed and discussed in Ref. 17 in the context of the FV semidiscretization of the governing flow equations. It requires the computation of a single convective flux per time step, whereas the approach summarized in Eq. (8) requires the computation at each time step of n_s convective fluxes.

Whether scheme (8) or (9) is chosen for extending the three-point backward difference scheme to moving grids, it remains to determine the number of mesh configurations n_s, the averaging coefficients c_s, the mesh configurations $\boldsymbol{x}_s$, and the mesh velocities $\dot{\boldsymbol{x}}_s$. To this effect, two approaches can be adopted. The first one consists in selecting the averaging parameters so that the resulting time integrator preserves the time accuracy of its fixed-grid counterpart. The second approach consists in choosing these parameters so that the resulting time integrator preserves the nonlinear stability of its fixed-grid counterpart.

It is proved in Refs. 20 and 21 that a necessary and sufficient condition for a given numerical scheme to preserve the nonlinear stability (in the sense of the discrete maximum principle) of its fixed-grid counterpart is to satisfy its corresponding discrete geometric conservation law (DGCL). From a physical viewpoint a DGCL ensures that an ALE or any other numerical scheme designed for solving unsteady flow problems on moving grids reproduces exactly a uniform flow. Hence, an ALE scheme that violates its DGCL is bound to exhibit spurious oscillations and overshoots for practical computational time steps. Occasionally, such a scheme can also exhibit an unbounded behavior. It is also shown in Ref. 21 that the extension to moving grids of the three-point backward difference scheme which satisfies the DGCL developed in Ref. 17 remains second-order accurate. For these reasons and because the computational overhead associated with enforcing a DGCL is minimal, numerical methods that satisfy their DGCLs should be preferred for CFD applications on moving grids.

B. Energy Conservative Exchange of Aerodynamic and Elastodynamic Data

In most practical cases the fluid and structure computational domains have nonmatching discrete interfaces. Let Γ_F and Γ_S denote the discrete representations of the fluid-structure interface Γ on the fluid and structure sides, respectively. The energy transferred from the fluid to the structure through Γ during the time-interval $[t^n, t^{n+1}]$ is

$$\delta\mathcal{E}_F^{n+1} = -\int_{t^n}^{t^{n+1}} \left[\int_\Gamma (-pn)\cdot \dot{x}\, \mathrm{d}s\right] \mathrm{d}t \tag{10}$$

and that received by the structure during the same time interval is

$$\delta\mathcal{E}_S^{n+1} = \int_{t^n}^{t^{n+1}} \left[\int_\Gamma (\sigma_S \cdot n)\cdot \dot{u}_S\, \mathrm{d}s\right] \mathrm{d}t \tag{11}$$

From the preceding expressions it follows that the discretization of the transmission conditions (2) and (3) has a direct impact on the

conservation of the energy transferred between the fluid and the structure through Γ.

Whichever approximation method (interpolation, projection, etc.) is chosen for enforcing on Γ the compatibility of the displacement fields of the fluid mesh and the structure [Eq. (3)], its outcome can be written as follows:

$$\boldsymbol{x}_j = \sum_{i=1}^{i_S} c_{ji} \boldsymbol{u}_{S_i}^P, \qquad j \in \Gamma_F, \qquad i \in \Gamma_S \tag{12}$$

where $\boldsymbol{x}_j$ is the discrete value of x at the fluid point j and $\boldsymbol{u}_{S_i}$ is the discrete value of u_S at the structure node i. The integer i_S and real coefficients c_{ji} depend on the chosen method of approximation. The superscript P is used to designate a "prediction" of the motion of the structure. If the fluid and structure subsystems are solved simultaneously, $\boldsymbol{u}_S^P = \boldsymbol{u}_S$. On the other hand, if they are advanced in time by a staggered procedure (see Sec. III.C) $\boldsymbol{u}_S^P$ will in general differ form $\boldsymbol{u}_S$ because of a time lag between the fluid and structure partitions.

Consider now a virtual displacement field $\hat{x}$ that is zero on each degree of freedom of the moving fluid grid except on those lying on the boundary Γ_F. Whichever method is chosen for approximating Eq. (1c) and therefore constructing the pseudostructural stiffness matrix $\tilde{\boldsymbol{K}}$, $\hat{x}$ can be expressed as follows:

$$\hat{x} = \sum_{j=1}^{j_F} D_j \hat{\boldsymbol{x}}_j, \qquad j \in \Gamma_F \tag{13}$$

where D_j is some function with a local or global support on Γ_F. From Eqs. (10) and (13) it follows that the virtual work during $[t^n, t^{n+1}]$ of the fluid tractions acting on Γ_F is

$$\delta W_F^{n+1} = \int_{t^n}^{t^{n+1}} \left[\sum_{j=1}^{j_F} \int_{\Gamma_F} (-pn) D_j \dot{\hat{\boldsymbol{x}}}_j \, \mathrm{d}s \right] \mathrm{d}t$$

$$= \int_{t^n}^{t^{n+1}} \sum_{j=1}^{j_F} \Phi_j \dot{\hat{\boldsymbol{x}}}_j \, \mathrm{d}t$$

where Φ_j has the physical meaning of a numerical pressure flux and is given by

$$\Phi_j = \int_{\Gamma_F} (-pn) \, D_j \, \mathrm{d}s \tag{14}$$

Substituting Eq. (12) into Eq. (14) gives

$$\delta W_F^{n+1} = \sum_{i=1}^{i_S} \int_{t^n}^{t^{n+1}} \boldsymbol{f}_{F_i} \dot{\hat{\boldsymbol{u}}}_{S_i}^P \, \mathrm{d}t \tag{15}$$

where

$$\boldsymbol{f}_{F_i} = \sum_{j=1}^{j_F} [\Phi_j][c_{ji}], \qquad j \in \Gamma_F, \qquad i \in \Gamma_S \tag{16}$$

If the nodal aerodynamic forces and moments acting on a structure node i lying on Γ_S are denoted by $\boldsymbol{f}_{S_i}^{\mathrm{ae}}$, the virtual work during $[t^n, t^{n+1}]$ of these forces is

$$\delta W_S^{n+1} = \int_{t^n}^{t^{n+1}} \sum_{i=1}^{i_S} \boldsymbol{f}_{S_i}^{\mathrm{ae}} \dot{\hat{\boldsymbol{u}}}_{S_i} \, \mathrm{d}t = \sum_{i=1}^{i_S} \int_{t^n}^{t^{n+1}} \boldsymbol{f}_{S_i}^{\mathrm{ae}} \dot{\hat{\boldsymbol{u}}}_{S_i} \, \mathrm{d}t \tag{17}$$

Conserving the transfer of energy through Γ requires enforcing $\delta W_F^{n+1} = \delta W_S^{n+1}$ for any pair of virtual displacement vectors $\hat{\boldsymbol{x}}$ and $\hat{\boldsymbol{u}}_S$ satisfying Eq. (12). From Eqs. (15) and (17) this implies enforcing

$$\int_{t^n}^{t^{n+1}} \boldsymbol{f}_{S_i}^{\mathrm{ae}} \dot{\hat{\boldsymbol{u}}}_{S_i} \, \mathrm{d}t = \int_{t^n}^{t^{n+1}} \boldsymbol{f}_{F_i} \dot{\hat{\boldsymbol{u}}}_{S_i}^P \, \mathrm{d}t \tag{18}$$

The evaluation of the time integrals in Eq. (18) depends on the time-integration schemes chosen for the structure and fluid analyzes and is discussed in great detail in Ref. 18. Here, we focus on the case where Eq. (5) is time integrated by the popular midpoint rule, which is second-order time accurate and in the linear case identical to the Newmark algorithm with $\beta = \frac{1}{4}$ and $\gamma = 1/2$ (Ref. 22), and Eq. (4) is time integrated with the second-order time accurate extension to moving grids of the three-point backward difference scheme described by Eq. (9). In this case Eq. (18) becomes

$$\left[\left(\boldsymbol{f}_{S_i}^{\mathrm{ae}\,n+1} + \boldsymbol{f}_{S_i}^{\mathrm{ae}\,n} \right) / 2 \right] \left(\boldsymbol{u}_{S_i}^{n+1} - \boldsymbol{u}_{S_i}^{n} \right)$$

$$= \left[\left(\boldsymbol{f}_{F_i}^{n+1} + \boldsymbol{f}_{F_i}^{n} \right) / 2 \right] \left(\boldsymbol{u}_{S_i}^{n+1^P} - \boldsymbol{u}_{S_i}^{n^P} \right) \tag{19}$$

If the fluid and structure subsystems are solved simultaneously, $\boldsymbol{u}_S^{n^P} = \boldsymbol{u}_S^n$, and Eq. (19) simplifies to

$$\boldsymbol{f}_{S_i}^{\mathrm{ae}} = \boldsymbol{f}_{F_i} = \sum_{j=1}^{j_F} [\Phi_j][c_{ji}], \qquad j \in \Gamma_F, \qquad i \in \Gamma_S \tag{20}$$

In this case Eq. (20) describes a conservative algorithm for transmitting the fluid forces to the structure. This algorithm is independent of the method chosen for discretizing the structure. The term in the first bracket in Eq. (20) depends exclusively on the method chosen for discretizing the flow problem, and the term in the second bracket depends only on the method selected for transmitting the displacement of the structure to the fluid mesh.

If a time lag is introduced in the solution of the fluid and structure subsystems, $\boldsymbol{u}_S^{n^P} \neq \boldsymbol{u}_S^n$. In this case conserving the energy transfer through Γ requires subiterating on $\boldsymbol{u}_S^{n^P}$ until $\boldsymbol{u}_S^{n^P} = \boldsymbol{u}_S^n$. Fortunately, subiterations are not necessary in practice because more computationally efficient means for compensating the strict loss of conservation of energy transfer through Γ are available and discussed in Sec. III.C.

C. Higher-Order Loosely Coupled Fluid-Structure Time Integrators

For any reasonably detailed FE representation of the aircraft structure, the simultaneous solution of Eqs. (1) by a monolithic scheme is neither practical nor software-wise manageable. For this and other reasons related to computational efficiency, a partitioned procedure is preferred for solving coupled field nonlinear aeroelastic problems. In such a procedure the fluid and structure are time integrated by different schemes tailored to their different mathematical models, and the resulting discrete equations are solved by a staggered algorithm.[7,8,23] Such a strategy simplifies explicit–implicit treatment, subcycling, load balancing, software modularity, and replacements as better mathematical models and methods emerge in the fluid and structure disciplines. The most popular partitioned procedure, which is referred to in this paper as the conventional serial staggered (CSS) procedure, can be described between t^n and t^{n+1} as follows: 1) predict $\boldsymbol{u}_S^{n+1^P} = \boldsymbol{u}_S^n$, transfer the corresponding motion of the wet boundary of the structure to the fluid subsystem, and update the position of the moving fluid mesh accordingly; 2) advance the fluid subsystem to t^{n+1} using a given flow time integrator and compute a new set of aerodynamic forces $\boldsymbol{f}_F^{n+1}$ acting on Γ_F; 3) transfer $\boldsymbol{f}_S^{\mathrm{ae}\,n+1} = \boldsymbol{f}_F^{n+1}$ to the structure subsystem; 4) apply $\boldsymbol{f}_S^{\mathrm{ae}\,n+1}$ to the structure and advance it to t^{n+1} using a given time integrator. Such a staggered procedure, which can be described as a loosely coupled solution algorithm, can also be equipped with a subcycling strategy where the fluid and structure subsystems are advanced using different time-steps Δt_F and Δt_S.

Unfortunately, the time accuracy of the CSS procedure is in general at least one order lower than that of its underlying flow and structure time integrators, and its numerical stability is more restrictive than that of the flow and structure solvers. Consequently, its maximum allowable time step is much smaller than required for accuracy purposes, which makes it a slow algorithm. To improve the performance of this simple partitioned procedure, several ad hoc strategies have been proposed in the literature. Essentially, these strategies insert some type of predictor–corrector iterations within each cycle of the computations in order to compensate for the time lag between the fluid and structure solvers.[23–25] These iterations help close the gap between $\boldsymbol{u}_S^{n+1^P}$ and $\boldsymbol{u}_S^{n+1}$ and conserve the transfer of energy between the fluid and structure through Γ.

As a result, they increase the maximum allowable time step of the CSS procedure. However, because the numerical complexity of each predictor–corrector iteration is almost the same as that of one cycle of staggering, little CPU is saved by such enhancement strategies.

Recently, Piperno and Farhat[18] have presented an alternative approach for improving the maximum allowable time step of the CSS procedure that does not increase the computational cost per cycle. Their approach is based on introducing two computationally economical factors for compensating the time lag between the fluid and the structure subsystems: 1) a nontrivial prediction $\boldsymbol{u}_S^{n+1^P} \neq \boldsymbol{u}_S^n$ and 2) a unnecessarily trivial transfer of the aerodynamic forces to the structure $\boldsymbol{f}_S^{\mathrm{ae}^{n+1}} \neq \boldsymbol{f}_F^{n+1}$. More specifically, they have shown that given two time-integration schemes for the fluid and structure equations of motion $\boldsymbol{u}_S^{n+1^P}$ and $\boldsymbol{f}_S^{\mathrm{ae}^{n+1}}$ can be designed to achieve

$$\sum_{n=0}^{NT/\Delta t} \delta W_F^n + \delta W_S^n = O(\Delta t^p) \tag{21}$$

where N is an arbitrary integer, T is the period of an assumed harmonic vibration of the structure, δW_F and δW_S are, respectively, the virtual work of the fluid and of the structure, and $\Delta t = \Delta t_F = \Delta t_S$ is a fixed time step for the fluid and structure time integrators. In other words, $\boldsymbol{u}_S^{n+1^P}$ and $\boldsymbol{f}_S^{\mathrm{ae}^{n+1}}$ can be designed to construct a p-order energy-transfer-accurate CSS procedure. The higher p is, the closer is the CSS procedure to conserving the transfer of energy through the fluid-structure interface. For example, consider the case where the CSS procedure is equipped with the midpoint rule[22] for time integrating the structure subsystem and the extension to moving grids of the three-point backward difference scheme for integrating the fluid subsystem. When $\boldsymbol{u}_S^{n+1^P} = \boldsymbol{u}_S^n$ and $\boldsymbol{f}_S^{\mathrm{ae}^{n+1}} = \boldsymbol{f}_F^{n+1}$, this CSS procedure is only first-order energy transfer accurate. On the other hand, if $\boldsymbol{u}_S^{n+1^P}$ is predicted by the following first-order scheme

$$\boldsymbol{u}_S^{n+1^P} = \boldsymbol{u}_S^n + (\Delta t_S/2)\dot{\boldsymbol{u}}_S^n \tag{22}$$

and the following "improved" vector of aerodynamic forces is applied on the wet surface of the structure

$$\boldsymbol{f}_S^{\mathrm{ae}^{n+1}} = 2\boldsymbol{f}_F^{n+1} - \boldsymbol{f}_S^{\mathrm{ae}^n} \tag{23}$$

the CSS procedure becomes third-order energy transfer accurate, and its maximum allowable time step is increased by a factor equal to five. This significant improvement in performance is achieved without any predictor–corrector iteration and almost at zero additional computational cost.

IV. Application to Prediction of Aeroelastic Parameters of an F-16 Configuration for Various Flight Conditions

The three-field-based nonlinear aeroelastic simulation technology just overviewed was first validated for the flutter analysis of the AGARD Wing 445.7 (Ref. 26). The remainder of this paper focuses on its further assessment for a full aircraft configuration and the preliminary assessment of its potential for complementing or replacing flutter testing of scaled models in transonic wind tunnels. More specifically, this section reports on the application of this aeroelastic simulation technology to the simulation of the flutter clearance of an F-16 Block-40 in clean wing configuration (e.g., no external stores) at the altitude of 3000 m and for $0.7 \leq M_\infty \leq 1.4$. For this purpose the authors have sought and obtained from Lockheed Martin modeling information for the structure of the F-16 Block-40. Using this information, they have assembled a detailed three-dimensional FE structural dynamic model of the F-16 Block-40 in clean wing configuration but with a launcher at each wing tip and two other launchers under each wing. This FE model features bar, beam, solid, plate, shell, metallic as well as composite elements, and contains a total of 168,799 dofs (Fig. 1a). It reproduces correctly, among others, the first dry bending and torsion frequencies that were evaluated in a ground vibration test at 4.76 and 7.43 Hz, respectively. The authors have also obtained F-16 CAD data from the U.S. Air Force Research Laboratory at Wright–Patterson AFB. Using these data and the ICEM CFD software, they have generated, after ignoring the presence of all launchers, a fluid volume mesh with 403,919 points, 63,044 of which are located on the surface of the aircraft (Fig. 1b).

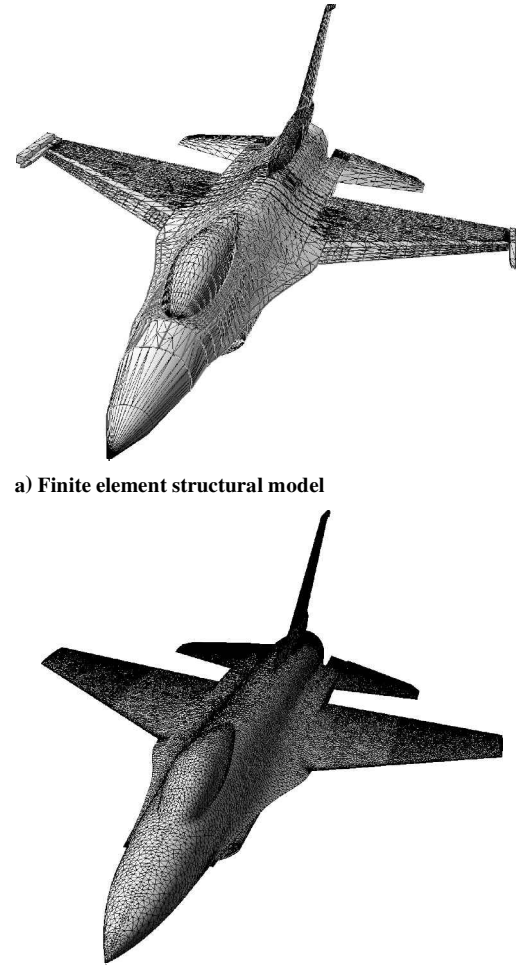

a) Finite element structural model

b) Fluid surface mesh

Fig. 1 F-16 Block-40: structural and fluid discretizations.

To perform a reasonably extensive assessment for this single F-16 Block-40 configuration, multiple aeroelastic simulations were performed using the AERO computational platform (see Sec. IV.A) developed at the University of Colorado for various stabilized, accelerated, low-g, and high-g flight conditions in subsonic, transonic, and supersonic airstreams. Figure 2 displays sample aeroelastic solutions obtained during these simulations. After these simulations were performed, the U.S. Air Force Test Pilot School (TPS) at the Edwards AFB performed a suite of flight tests in order to generate validation data for various flight conditions including those simulated by the AERO software platform. More specifically, the TPS flew an F-16 Block-40 fighter in clean wing configuration but equipped with one launcher at each wing tip and two launchers under each wing to accommodate instrumentation. The Flight Test Center at the Edwards AFB postprocessed the flight-test data for the first aeroelastic torsional mode only and provided the results to the authors for the purpose of correlation.

In addition to presenting the results of the correlation effort just described, the following sections comment on the influence on the aeroelastic behavior of a fighter of various flight parameters such as loading and acceleration.

A. AERO Simulation Platform

The AERO-F, AERO-S, and MATCHER codes developed at the University of Colorado are a suite of software modules based on the three-field formulation described in this paper for the solution on nonlinear transient aeroelastic problems. They are portable and run on a large variety of computing platforms ranging from Unix workstations to shared as well as distributed memory massively parallel computers.

a) Von Mises stresses (amplified aeroelastic deformations)

b) Mach contours (amplified aeroelastic deformations)

Fig. 2 F-16 Block-40: sample solutions at $M_\infty = 0.9$ and $t = 0.6\,s$.

The three-dimensional AERO-F module models a flow either by the Euler equations or by the averaged Navier–Stokes equations equipped with the k-ε[27] or Spalart–Allmaras[28] turbulence model and a wall function.[29] It operates on static and dynamic unstructured meshes. More specifically, it combines a Galerkin-centered approximation for the viscous terms and a Roe upwind scheme for the convective fluxes. Higher-order spatial accuracy is achieved through the use of a multidimensional piecewise linear reconstruction that follows the principle of the Monotonic Upwind Scheme for Conservative Laws.[30] Time integration on moving grids is carried out as described in Sec. III.A. All linearized systems of equations are solved by the Restricted Additive Schwarz Preconditioned Generalized Minimum Residual (GMRES) Iterative Algorithm.[31] The AERO-F module supports a robust structure analogy method for constructing dynamic meshes that is based on time-dependent torsional springs.[32] The main purpose of these springs is to provide each fluid mesh element a fictitious stiffness, which increases to infinity when the volume of that element decreases to zero. This prevents all collapsing mechanisms (node-to-node, node-to-edge, and node-to-face) from occurring during the mesh motion.

The AERO-S structural code is capable of linear and geometrically nonlinear static, sensitivity, vibration, and transient FE analyses of restrained as well as unrestrained homogeneous and composite structures.

The AERO-F and AERO-S codes communicate via run time MPI software channels. They exchange aerodynamic and elastodynamic data across nonmatching fluid and structure mesh interfaces as described in Sec. III.B. For this purpose they are guided by information generated in a preprocessing phase by the MATCHER software.[33]

B. Numerical Excitation and Parameter Identification

To determine the frequency f_{tor} and damping coefficient α_{tor} of the first aeroelastic torsional mode of the target F-16 configuration, the following procedure was adopted. For each flight condition the structure was excited by a symmetric initial disturbance, and its response to that disturbance was simulated. Once the signals were generated for a sufficiently long period of time, the Eigensystem Realization Algorithm (ERA)[34] was applied to extract from them the aeroelastic parameters f_{tor} and α_{tor}. Focus was set on the vertical displacement dofs at one root node of each wing. This corresponds to positioning output sensors at these locations for flight testing.

The ERA is a real-time parameter identification method that is less sensitive to noise than the classical logarithmic decay method. It can handle multi-input multi-output (multi-degree-of-freedom) systems. Most importantly, it is capable of identifying the frequencies and damping coefficients of the two lowest dominating modes of a structure using as few as three cycles of response history, as long as the sampling rate is on the order of 500–1000 Hz ($\Delta t = 1$ to 2 ms).[35] Hence, it is particularly attractive to time-domain aeroelastic applications. In this work ERA was fed with two to four cycles of the simulated vibration of the F-16 structure to extract the sought-after aeroelastic parameters in stabilized, accelerated, and loaded flight conditions.

C. Stabilized Flight Conditions

In this series of simulations, the freestream Mach number was fixed throughout the structural vibrations. Figure 3a reports a good agreement between the simulation results and flight-test data, including in the transonic regime. The maximum relative discrepancy between these two sets of data is 7% for the wet frequency f_{tor} and 14% for the wet damping coefficient α_{tor}. More important, Fig. 3a shows that the AERO code reproduces correctly the variation of the aeroelastic torsional damping coefficient with the Mach number.

D. Accelerated Flight Conditions

It has been suggested that flutter testing could be performed in accelerated flight in order to reduce the cost of determining the flutter envelopes of fighters.[35] It also appears that this idea has been occasionally implemented in some flight-test programs. Such a procedure raises the fundamental issue of how to relate the aeroelastic parameters measured in an accelerated flight to those measured in stabilized flight conditions. This issue was addressed in Ref. 35 by a mathematical analysis of the typical wing section in level flight. The results of this two-dimensional analysis suggest that any realistic acceleration should not affect the aeroelastic frequencies and damping ratios of an aircraft. To verify these analytical results, several simulations were performed for the F-16 configuration described in this paper in accelerated flight conditions. To simulate an accelerated flow, the motion of the moving fluid grid was accelerated, and its position was updated as follows:

$$\bar{x}^n = x^n + 0.5\,a t^{n^2} \tag{24}$$

where x denotes as before the position of a moving fluid grid point in the absence of acceleration, a denotes a constant acceleration in the direction of flight, and $\bar{x}$ denotes the position of a moving fluid grid point caused by both the vibration of the aircraft and its acceleration. This acceleration was set to 0.02 Mach per second, which is typical for an F-16 in level flight.

The numerical results reported in Fig. 3a show that this level acceleration does not have a significant impact on the aeroelastic frequency and damping coefficient of the first torsional mode, which corroborates the results of the two-dimensional mathematical analysis presented in Ref. 35.

E. High-g Flight Conditions

Finally, another series of aeroelastic simulations were performed for stabilized flight conditions but with 3.5g and 5g load factors. During flight test, these load factors were achieved by level-flight turns. In the simulations these load factors were reproduced by adjusting the angle of attack. For example, at Mach 1 angles of attack of 3 and 4 deg reproduce 3.5g and 5g flight conditions. At lower Mach numbers the adjusted angle of attack can be as high as 13 deg.

Figures 3b and 3c show that, in general, the numerical results generated by the AERO simulation platform are in good agreement with the flight-test data. For both cases of 3.5*g* and 5*g* load factors, the maximum discrepancy between the simulated and measured aeroelastic torsional frequency is 2%. The maximum discrepancy for the aeroelastic torsional damping ratio is 20% (except for an outlier point for the 3.5*g* case). However, in both cases the AERO code reproduces correctly the trend of the variation of the aeroelastic torsional damping coefficient with the Mach number.

Furthermore, the flight-test data suggest that f_{tor} increases with the load factor (Fig. 4). No conclusion is formulated as for the effect on α_{tor} of a higher load factor because the corresponding flight-test data do not suggest any specific trend (Fig. 4). Perhaps, this is caused by the significant oscillations of the angle of attack that were observed during the flight test for both 3.5*g* and 5*g* flight conditions.

V. Practical Feasibility

Finally, the speed of the nonlinear aeroelastic simulation technology described in this paper is discussed, particularly in the context of this second quote from Ref. 5: "Even at present, existing CFD codes should be able to obtain five flutter solutions in one year."

For the F-16 configuration considered herein, the AERO simulation platform sustains a coupling time step on the order of 1 ms. This time step corresponds to sampling the period of the first dry torsional mode of this fighter by 134 points. It also turns out that this time step is such that about 400 time steps are needed to simulate the first three cycles of the structural response to an initial disturbance.

The performance results obtained on an SGI Origin 3200 computer equipped with R12000 400 MHz CPUs are reported in Table 1 as a function of the number of processors N_{proc} allocated to the flow solver AERO-F. These results correspond to a single Mach-number point and three cycles of the response of the structure. In all cases a

Table 1 F-16 Block-40: performance results on an Origin 3200 for a single Mach-number point and three cycles of the response of the structure (400 coupling time steps)

N_{proc} fluid	CPU total, h	CPU fluid, %	CPU mesh, %	CPU structure, %	Parallel speed-up	Parallel efficiency, %
1	52.3	62.4	37.4	0.2	1.0	100
3	18.4	64.6	34.8	0.6	2.8	95
6	9.6	63.3	35.4	1.3	5.4	91
12	4.4	57.1	40.1	2.8	11.9	99
24	2.5	52.7	42.7	4.6	20.9	87

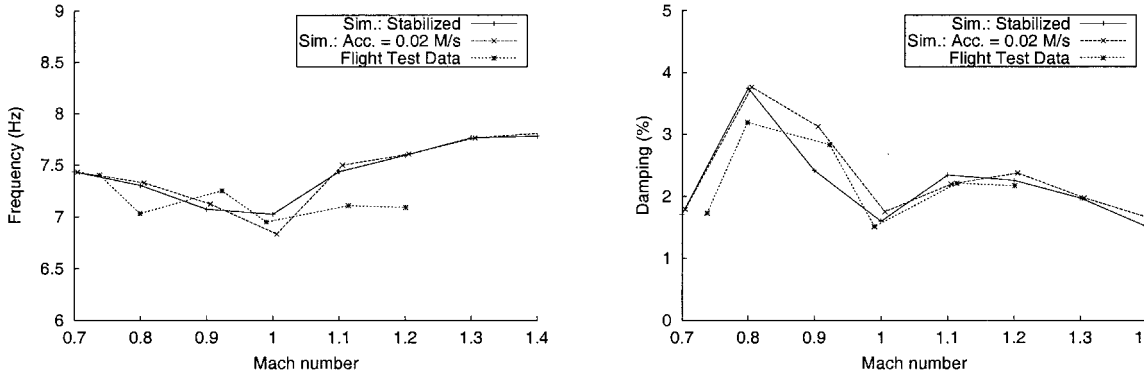

a) Stabilized and accelerated flight conditions

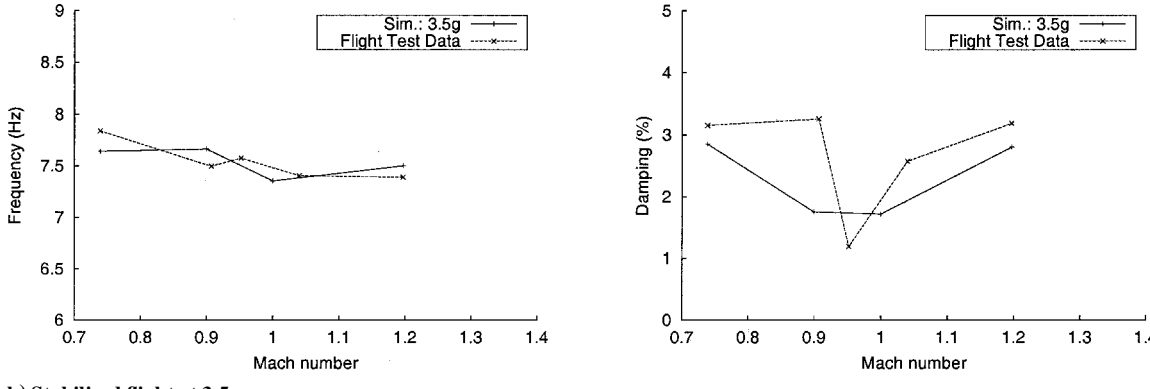

b) Stabilized flight at 3.5*g*

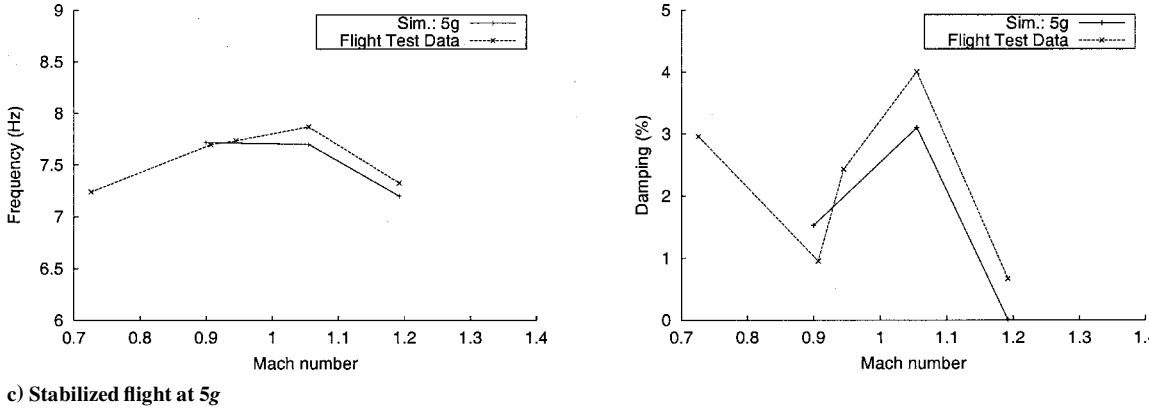

c) Stabilized flight at 5*g*

Fig. 3 F-16 Block-40: aeroelastic parameters (first torsional mode) at the altitude of 3000 m.

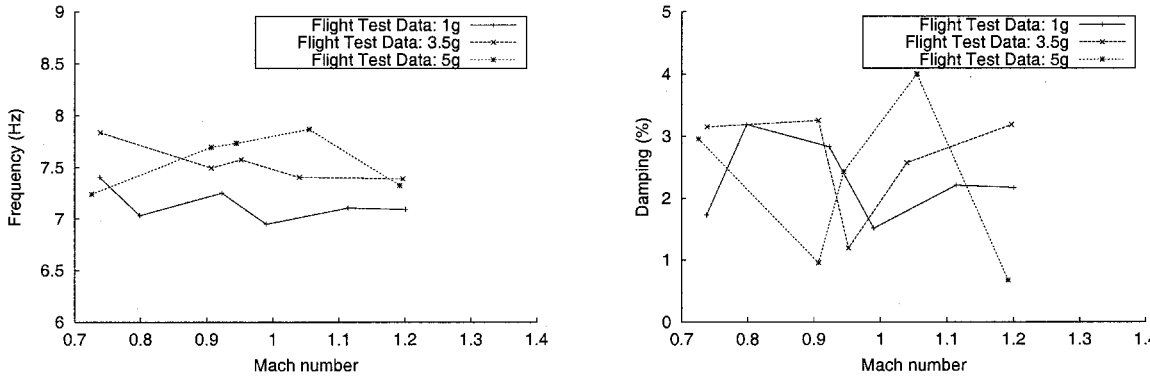

Fig. 4 F-16 Block-40: effect of the load factor on the first torsional aeroelastic frequency and damping coefficient.

single processor is assigned to the structure solver AERO-S because it is less computationally intensive than the flow and mesh motion solvers. The reader can observe that on average 60% of the total CPU time is elapsed in AERO-F, 38% in the mesh motion solver, which is embedded in AERO-F, and only 2% in AERO-S. The small percentage of the CPU time consumed by the structure solver is from the assumed linear nature of the structural problem in this case.

The parallel speed-up and parallel efficiency results reported in Table 1 highlight the good parallel scalability of the AERO simulation platform. One can reasonably argue that today most aerospace engineers have access to a six-processor computational platform. From the results reported in Table 1, it can be concluded that using such a computing system the transonic aeroelastic parameters of a full fighter configuration can be extracted in 9.6 h. For a given Mach number finding the flutter speed usually requires a bracketing procedure. It is the authors' experience that such a bracketing procedure typically incurs about five simulations that are similar to the one discussed herein. Hence, for a given Mach number the flutter speed requires about 48 h CPU on a six-processor computational platform. Therefore, five flutter point solutions for a fighter in the transonic regime can be obtained in less than 10 days. It is the authors' experience that five flutter point solutions for a fighter in the transonic regime can be obtained with AERO in two days when computing on a 40-processor Origin 3200.

VI. Conclusions

High-performance military aircraft are usually flutter critical in the transonic regime where the linear flow theory fails to predict correctly the unsteady aerodynamic forces acting on an aircraft. Consequently, flutter testing of scaled models in transonic wind tunnels is always used to generate corrections to flutter speeds predicted by linear methods. Because the design of a wind-tunnel flutter model and the analysis of the corresponding data require over a year's time, it has been suggested that computational-fluid-dynamics-based nonlinear aeroelastic simulations could be used as a replacement for wind-tunnel testing if they prove to be practical, that is, fast enough, and reliable.[5]

The authors believe that the nonlinear aeroelastic simulation methodology presented in this paper is today sufficiently mature to take on this challenge. At the present time it might not be sufficiently fast to be used as a design tool. However, as reported in this paper this nonlinear aeroelastic simulation technology, and perhaps other similar ones, are capable of computing in the inviscid case five flutter point solutions for a fighter in the transonic regime in less than 10 days on a six-processor computing platform. When applied to an F-16 fighter in clean wing configuration and various stabilized, accelerated and increased angle-of-attack flight conditions, it produced aeroelastic numerical results that are in good agreement with flight-test data. Furthermore, these inviscid simulation results suggest that the level acceleration achievable by an F-16 does not have a significant impact on its aeroelastic parameters. They also indicate that a higher loading caused by an increased angle of attack tends to increase the aeroelastic torsional frequency. Future work will focus on including viscous effects in the flow model in order to properly address limit-cycle oscillations and buffet phenomena.

Acknowledgments

The authors acknowledge the support by the U.S. Air Force Office of Scientific Research under Grant F49620-01-1-0129. They thank Tracy Redd and Paul Waters from the U.S. Air Force Flight Test Center at the Edwards Air Force Base for providing them the F-16 flight test data. They also thank ICEM CFD Engineering, Inc., for providing their mesh generation software.

References

[1]Dat, R., and Meurzec, J. L., "Sur les Calculs de Flottement par la Méthode Dite du "Balayage" en Fréquence Réduite," *La Recherche Aérospatiale*, Vol. 133, 1969.

[2]Hassig, H. J., "An Approximate True Damping Solution of the Flutter Equation by Determinant Iteration," *Journal of Aircraft*, Vol. 8, No. 11, 1971, pp. 885–889.

[3]Albano, E., and Rodden, W. P., "A Doublet-Lattice Method for Calculating Lift Distribution on Oscillating Surfaces in Subsonic Flow," *AIAA Journal*, Vol. 7, No. 2, 1969, pp. 279–285.

[4]Ashley, H., and Zartarian, G., "Piston Theory—A New Aerodynamic Tool for the Aeroelastician," *Journal of the Aeronautical Sciences*, Vol. 23, 1956, pp. 1109–1118.

[5]Yurkovich, R. N., Liu, D. D., and Chen, P. C., "The State-of-the-Art of Unsteady Aerodynamics for High Performance Aircraft," AIAA Paper 2001-0428, 2001.

[6]Lee-Rausch, E. M., and Batina, J. T., "Wing-Flutter Boundary Prediction Using Unsteady Euler Aerodynamic Method," AIAA Paper 93-1422, 1993.

[7]Farhat, C., Lesoinne, M., and Maman, N., "Mixed Explicit/Implicit Time Integration of Coupled Aeroelastic Problems: Three-Field Formulation, Geometric Conservation and Distributed Solution," *International Journal for Numerical Methods in Fluids*, Vol. 21, 1995, pp. 807–835.

[8]Gupta, K. K., "Development of a Finite Element Aeroelastic Analysis Capability," *Journal of Aircraft*, Vol. 33, No. 5, 1996, pp. 995–1002.

[9]Sheta, E., and Huttsell, L., "Numerical Analysis of F/A-18 Vertical Tail Buffeting," AIAA Paper 2001-1664, 2001.

[10]Melville, R., Morton, S., and Rizzetta, D., "Implementation of a Fully-Implicit Aeroelastic Navier–Stokes Solver," AIAA Paper 97-2039, 1997.

[11]Guruswamy, G., and Byun, C., "Direct Coupling of Euler Flow Equations with Plate Finite Element Structures," *AIAA Journal*, Vol. 33, No. 2, 1995, pp. 375–377.

[12]Lesoinne, M., and Farhat, C., "Stability Analysis of Dynamic Meshes for Transient Aeroelastic Computations," AIAA Paper 93-3325, 1993.

[13]Bhatia, K. G., "Airplane Aeroelasticity: Practice and Potential," AIAA Paper 2001-0430, 2001.

[14]Donea, J., "An Arbitrary Lagrangian-Eulerian Finite Element Method for Transient Fluid-Structure Interactions," *Computer Methods in Applied Mechanics and Engineering*, Vol. 33, 1982, pp. 689–723.

[15]Batina, J. T., "Unsteady Euler Airfoil Solutions Using Unstructured Dynamic Meshes," AIAA Paper 89-0115, 1989.

[16]Lesoinne, M., and Farhat, C., "Geometric Conservation Laws for Flow Problems with Moving Boundaries and Deformable Meshes and Their Impact on Aeroelastic Computations," *Computer Methods in Applied Mechanics and Engineering*, Vol. 134, 1996, pp. 71–90.

[17]Koobus, B., and Farhat, C., "Second-Order Time-Accurate and Geometrically Conservative Implicit Schemes for Flow Computations on Unstructured Dynamic Meshes," *Computer Methods in Applied Mechanics and Engineering*, Vol. 170, 1999, pp. 103–130.

[18]Piperno, S., and Farhat, C., "Partitioned Procedures for the Transient Solution of Coupled Aeroelastic Problems—Part II: Energy Transfer Analysis and Three-Dimensional Applications," *Computer Methods in Applied Mechanics and Engineering*, Vol. 190, 2001, pp. 3147–3170.

[19]Farhat, C., *High Performance Simulation of Coupled Nonlinear Transient Aeroelastic Problems*, Special Course on Parallel Computing in CFD, von Kármán Inst., AGARD R-807, Brussels, Oct. 1995, Chap. 7.

[20]Farhat, C., Geuzaine, P., and Grandmont, C., "The Discrete Geometric Conservation Law and the Nonlinear Stability of ALE Schemes for the Solution of Flow Problems on Moving Grids," *Journal of Computational Physics*, Vol. 174, 2001, pp. 669–694.

[21]Farhat, C., Geuzaine, P., and Grandmont, C., "The Discrete Geometric Conservation Law and Its Effects on Nonlinear Stability and Accuracy," AIAA Paper 2001-2607, 2001.

[22]Hughes, T. J. R., "Analysis of Transient Algorithms with Particular Reference to Stability Behavior," *Computational Methods for Transient Analysis*, edited by T. Belytschko and T. Hughes, North-Holland, Amsterdam, 1983, pp. 67–155.

[23]Strganac, T. W., and Mook, D. T., "Numerical Model of Unsteady Subsonic Aeroelastic Behavior," *AIAA Journal*, Vol. 28, No. 5, 1990, pp. 903–909.

[24]Pramono, E., and Weeratunga, S. K., "Aeroelastic Computations for Wings Through Direct Coupling on Distributed-Memory MIMD Parallel Computers," AIAA Paper 94-0095, 1994.

[25]Mouro, J., "Numerical Simulation of Nonlinear Fluid Structure Interactions Problems and Application to Hydraulic Shock-Absorbers," *Proceedings of the Third World Conference in Applied Computational Fluid Dynamics*, World User Days CFD, Basel, 1996.

[26]Lesoinne, M., and Farhat, C., "Higher-Order Subiteration-Free Staggered Algorithm for Nonlinear Transient Aeroelastic Problems," *AIAA Journal*, Vol. 36, No. 9, 1998, pp. 1754–1756.

[27]Jones, W. P., and Launder, B. E., "The Prediction of Laminarization with a Two-Equation Turbulence Model," *International Journal of Heat and Mass Transfer*, Vol. 15, 1972, pp. 301–314.

[28]Spalart, P. R., and Allmaras, S. R., "A One-Equation Turbulence Model for Aerodynamic Flows," AIAA Paper 92-0439, 1992.

[29]Wilcox, D. C., *Turbulence Modeling for CFD*, DCW Industries, La Canada, CA, 1993.

[30]Dervieux, A., "Steady Euler Simulations Using Unstructured Meshes," *Proceedings of the VKI Lectures Series 1985-04*, von Kármán Inst., Brussels, 1985.

[31]Cai, X. C., Farhat, C., and Sarkis, M., "A Minimum Overlap Restricted Additive Schwarz Preconditioner and Applications in 3D Flow Simulations," *Contemporary Mathematics*, Vol. 218, 1998, pp. 478–484.

[32]Degand, C., and Farhat, C., "A Three-Dimensional Torsional Spring Analogy Method for Unstructured Dynamic Meshes," *Computers and Structures*, Vol. 80, 2001, pp. 305–316.

[33]Maman, N., and Farhat, C., "Matching Fluid and Structure Meshes for Aeroelastic Computations: A Parallel Approach," *Computers and Structures*, Vol. 54, No. 4, 1995, pp. 779–785.

[34]Juang, J. N., and Pappa, R. S., "An Eigensystem Realization Algorithm (ERA) for Modal Parameter Identification and Model Reduction," *Journal of Guidance, Control, and Dynamics*, Vol. 8, No. 5, 1985, pp. 620–627.

[35]Farhat, C., and Harris, C., and Rixen, D., "Expanding a Flutter Envelope Using Accelerated Flight Data: Application to an F-16 Fighter Configuration," AIAA Paper 2000-1702, 2000.

E. Livne
Associate Editor